Continuous Phase Control of Vanadium Dioxide Films

Jiguo Dai
Department of Mechanical Engineering,
Texas Tech University,
Lubbock, TX 79409
e-mail: jiguo.dai@ttu.edu

Chandika Annasiwatta
Department of Physics and Engineering,
Muskingum University,
New Concord, OH 43762
e-mail: annasi@muskingum.edu

Ayrton Bernussi
Department of Electrical & Computer Engineering and
Nano Tech Center,
Texas Tech University,
Lubbock, TX 79409
e-mail: ayrton.bernussi@ttu.edu

Zhaoyang Fan
Department of Electrical & Computer Engineering and
Nano Tech Center,
Texas Tech University,
Lubbock, TX 79409
e-mail: zhaoyang.fan@ttu.edu

Jordan M. Berg
Division of Civil, Mechanical, and Manufacturing Innovation,
U.S. National Science Foundation,
Alexandria, VA 22314
e-mail: jberg@nsf.gov

Beibei Ren[1]
Department of Mechanical Engineering,
Texas Tech University,
Lubbock, TX 79409
e-mail: beibei.ren@ttu.edu

Vanadium dioxide (VO_2) undergoes a metal-insulator transition (MIT) at approximately 68 °C, with associated sharp changes in its physical (e.g., optical, electrical, and mechanical) properties. This behavior makes VO_2 films of interest in many potential applications, including memory devices, switches, sensors, and optical modulators. For ON/OFF like digital applications, an abrupt switching behavior is ideal. However, to continuously change VO_2 metal/insulator phase ratio for analog-like operation, the intrinsic hysteresis characteristic of VO_2 MIT renders the phase control becoming a formidable challenge. This paper considers the problem of controlling and tracking desired optical transmittance via continuous phase ratio change. The problem becomes worse while considering the differences of individual thin-film samples and the hysteresis associated with the phase change within a narrow temperature range. This paper reports a robust feedback controller using an optical transmittance measurement and based on an uncertainty and disturbance estimator (UDE) architecture. The proposed controller is capable of mitigating the adverse effect of hysteresis, while also compensating for various uncertainties. The effectiveness of the proposed methodology is demonstrated with experimental validation.
[DOI: 10.1115/1.4046929]

Keywords: phase control, vanadium dioxide (VO_2), uncertainty and disturbance estimator (UDE)

1 Introduction

It is well known that vanadium dioxide (VO_2) undergoes a thermally induced metal-insulator transition (MIT) around 68 °C [1,2]. Its physical (e.g., optical, electrical, and mechanical) properties inherit significant changes when the temperature varies across the MIT region. Due to this attribute, VO_2 has become a promising functional material in micro-actuation [3], sensors [4], memory [5], optical devices [6], etc.

However, the MIT of VO_2 exhibits hysteresis, i.e., the variation of certain physical properties (transmittance, resistance, mechanical stress, etc.) when the external driving factors (thermal temperature, voltage, etc.) change, also depends on the phase transition history. Therefore, the intermediate values in the MIT region cannot be attained reliably by simple control of the driving factors. As a result, the application of VO_2 is limited to the ON/OFF binary mode, like in electric switches [7] or optical switches [8], thus avoiding the MIT region. A temperature can be used to trigger the phase transition, leading from a high-resistance/transmittance to a low-resistance/transmittance, i.e., inducing the switching behavior. However, the applicability of VO_2 stands to be broadened into the "analog" mode if the intermediate states within the phase transition region could be controlled.

Chemical doping has been used to modify the MIT property of VO_2 as reported in Refs. [9] and [10]. Specifically, doping can change the phase transition abruptness, and thus, the variation of a given physical property with the external driving factor will slow down. Subsequently, the control of the physical property within the phase transition can be made easier. In Ref. [11], by modifying the concentration of tungsten (W) for W-doped VO_2, the gradual controlling of the MIT region can be achieved. However, this control is achieved by sacrificing the modulation depth. This is not desirable because the performance of many tunable devices is critically dependent on the modulation depth. Furthermore, the nonunique relationship between the controlled property value and the driving factor still exists as the MIT hysteresis cannot be eliminated.

Therefore, achieving the precise phase controlling for a VO_2 film with a high modulation depth is a challenging problem. This work aims to incorporate the feedback mechanism into the VO_2 device and achieve the precise phase controlling within the full operational range of the VO_2 films. To tackle with the severe hysteresis nonlinearity as well as the various uncertainties, both model-based and nonmodel-based control methodologies have been investigated in the literature. For the model-based control, a hysteresis model is required and an inverse hysteresis model is then implemented to minimize the hysteresis effect. For example, the Preisach model was studied in Ref. [12] to describe the hysteresis phenomenon of optical and electric properties of VO_2 films. In Refs. [3] and [13], the generalized Prandtl–Ishlinskii model was investigated for VO_2 based actuators. However, such hysteresis models are always mathematically complicated and highly sensitive to system parameters. These bring new challenges for the model-based control methodologies. Therefore, a nonmodel-based controller that is easily implementable and does not rely as much on the hysteresis model information is preferred. In Ref. [14], a

[1]Corresponding author.

Contributed by the Dynamic Systems Division of ASME for publication in the Journal of Dynamic Systems, Measurement, and Control. Manuscript received April 22, 2019; final manuscript received March 31, 2020; published online May 11, 2020. Assoc. Editor: Bin Xian.

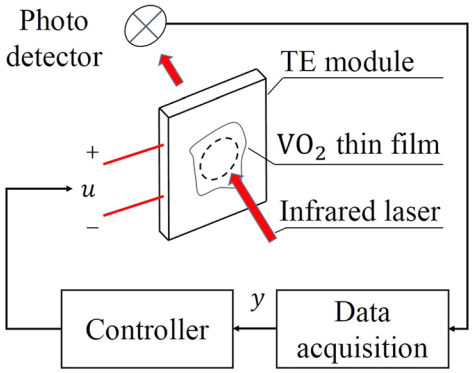

Fig. 1 System configuration

classical proportional-integral (PI)-type controller is applied to control an VO_2 integrated micro-actuator. Compared to the PI controller, a novel robust controller, named uncertainty and disturbance estimator (UDE)-based robust control [15–18], was shown having a superior robust performance and successfully applied to many practical systems. The main advantage of this robust control methodology is that it can achieve an excellent performance while using limited system model information. Therefore, this paper adopts the UDE-based robust control for precise phase controlling of VO_2 films, where the optical transmittance is considered as the controlled property.

Once the proposed robust feedback control mechanism achieves the precise phase controlling of VO_2 within its full operational range, the overall closed-loop system can be regarded as a VO_2 device with a reconfigurable phase transition region. All the intermediate states within the phase transition region can then be treated as operational states. Continuous phase controlling can enable VO_2 for many analog applications [6].

2 Modeling

Figure 1 illustrates the system configuration where a VO_2 thin film deposited on a sapphire substrate is heated or cooled by using a thermoelectric (TE) module. The optical transmittance of the VO_2 thin film, $y(\%)$, can be tuned by the temperature of the VO_2 thin film, $v(^\circ\text{C})$, which can be controlled by changing the input voltage signal $u(V)$ of the TE module. The optical transmittance y is measured by a photodetector and fed back into a controller for the control purpose. The mathematical model of the system can be described by a linear first-order differential equation connected in series with a hysteresis operator

$$T\frac{dv}{dt} = -v + Ku + \delta \tag{1}$$

$$y = \Phi[v] \tag{2}$$

where T (s) is the time constant, K (°C/V) is the static gain, δ (°C) represents the effect of various uncertainties and disturbances on the temperature channel, and $\Phi[\cdot]$ (°C → %) is the hysteresis operator, which can be described by different mathematical models, e.g., the Preisach model [12], generalized Prandtl–Ishlinskii model [13], etc.

3 Proposed Feedback Control Architecture

3.1 The Empowered VO_2 Device. The proposed concept of the empowered VO_2 device is illustrated in Fig. 2. The empowered VO_2 device contains two virtual components to be designed, especially, the reference model and the feedback controller.

3.1.1 Reference Model Design. The purpose of proposing a reference model is to formulate a desired input–output relationship for the empowered VO_2 device. The reference model gives a

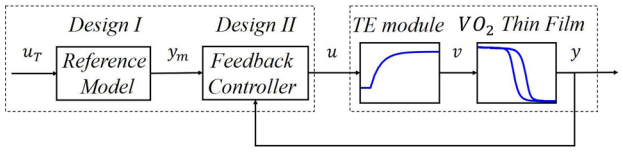

Fig. 2 Concept of an empowered VO_2 device with the reconfigurable phase transition

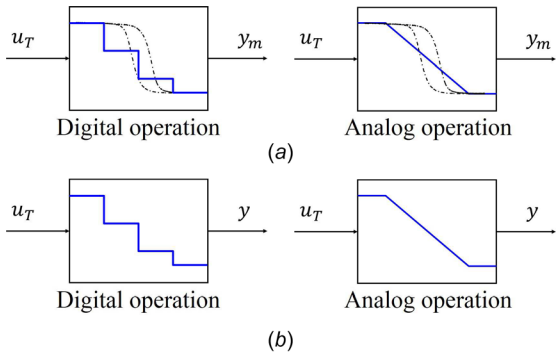

Fig. 3 Concept of the reference model and the closed-loop system behavior: (*a*) the reference model and (*b*) desired behavior for the closed-loop system

new one-to-one relationship, $H_m : u_T \rightarrow y_m$, between a regulation signal u_T and a reference signal y_m. H_m explicitly expresses the reconfigurable phase transition, which is determined by the application demand. The reference model can be either digital-like or analog-like as shown in Fig. 3(*a*). For example, y_m can have distinct values while the reference model behaves as a multiple-state toggle switch. For each specific range of u_T, a desired value of y_m is assigned. Moreover, if the reference model is applied as a tuning knob, the values of both y_m and u_T are then continuously spanned over an interval. In this case, the reference signal y_m can be continuously tuned by changing the value of u_T. The reference signal y_m should be physically feasible, which is achievable by the VO_2 thin film.

3.1.2 Feedback Controller Design. The design of the feedback controller plays a key role in the empowered VO_2 device. The objective of the feedback controller is to regulate the system output y to the reference signal y_m precisely and quickly. As shown in Fig. 3(*b*), once the precise regulation is achieved, the closed-loop system will behave like the desired reference model. Consequently, the empowered VO_2 device would have a reconfigurable phase transition to fulfill the application demand. The challenges for the controller design are listed as follows: (1) the severe hysteresis effect associated with the phase change and (2) the unknown system uncertainties and disturbances. Let $e = y_m - y$ define the tracking error, the feedback controller aims to control the cascaded system (1) and (2) to achieve the following error dynamics:

$$\dot{e} = -ke \tag{3}$$

where the error feedback gain $k > 0$ tunes the convergence rate of e, i.e., $\lim_{t\to\infty} e(t) = \lim_{t\to\infty} e(0)\exp(-kt) = 0$.

3.2 Model Order Reduction. Following the idea in Ref. [18], an equivalent transformation is introduced to facilitate the controller design as shown in Fig. 4. The original system (1) and (2) is easily verified to be a bounded-input-bounded-output system, and also Lipschitz smooth, which are required by this approach [18].

As shown in Fig. 4(*b*), a proper first-order linear system $(b/(s+a))$ is introduced, where $a > 0$ and b has the same sign as the system static gain. The equivalent transferred system becomes

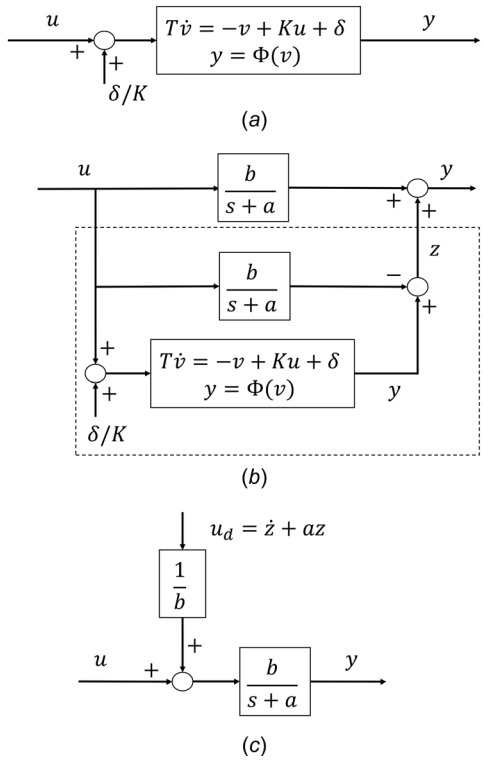

Fig. 4 Concept of the equivalent transformation for the controller design [18]: (*a*) the original system, (*b*) the introduction of a first-order linear system, and (*c*) the equivalent system

a first-order linear system plus a lumped uncertainty term as shown in Fig. 4(*c*). There is

$$y = \mathcal{L}^{-1}\left\{\frac{b}{s+a}\right\} * u - \mathcal{L}^{-1}\left\{\frac{b}{s+a}\right\} * u + y = \mathcal{L}^{-1}\left\{\frac{b}{s+a}\right\} * u + z \tag{4}$$

where "$*$" is the convolution operator, $\mathcal{L}^{-1}\{\cdot\}$ is the inverse Laplace operator, and $z = y - \mathcal{L}^{-1}\{(b/(s+a))\} * u$. Furthermore, Eq. (4) becomes

$$\dot{y} = -ay + bu + \dot{z} + az = -ay + bu + u_d \tag{5}$$

where $u_d = \dot{z} + az$ is the lumped uncertainty term including the contribution of the (unknown) dynamics, hysteresis, and disturbances of the system. After the transformation, the system model order is reduced as a first-order linear system with a lumped uncertainty term. The major advantage of this approach is the relaxation of the modeling process of the hysteresis nonlinearity $\Phi[v]$ in Eq. (2).

3.3 Feedback Controller Based on Uncertainty and Disturbance Estimator. Combining Eqs. (3) and (5) leads to the controller

$$u = \frac{1}{b}[\dot{y}_m + ke + ay - u_d] \tag{6}$$

From Eq. (5), there is $u_d = \dot{y} + ay - bu$. Based on the key idea of the UDE-based robust control [15], u_d can be estimated with a strictly proper and stable filter $G_f(s)$ as

$$\hat{u}_d = g_f(t) * u_d = g_f(t) * (\dot{y} + ay - bu) \tag{7}$$

where $g_f(t) = \mathcal{L}^{-1}\{G_f(s)\}$ is the impulse response of the filter $G_f(s)$. If this filter has the unity gain and zero phase shift over the spectrum of u_d and zero gain elsewhere, then the estimation (7) is accurate [17]. By replacing u_d in Eq. (6) with $\hat{u}_d$ in Eq. (7), the UDE-based robust feedback controller can be obtained as

$$u = \frac{1}{b}\left[ay - \mathcal{L}^{-1}\left\{\frac{sG_f(s)}{1-G_f(s)}\right\} * y + \mathcal{L}^{-1}\left\{\frac{1}{1-G_f(s)}\right\} * (\dot{y}_m + ke)\right] \tag{8}$$

The overall closed-loop system is demonstrated in Fig. 5. More details about the proposed control methodology including the parameter selection and stability analysis can be found in Ref. [18].

3.4 Performance Analysis. Assume that the lumped uncertainty term u_d varies slowly too. The low-pass filter in the controller (8) can be chosen as $G_f(s) = (1/(\tau s + 1))$, where $\tau > 0$ is the time constant. The guideline of selecting the time constant τ is to ensure the bandwidth of the filter $G_f(s)$ cover the spectrum of u_d. The error dynamics for the overall closed-loop system is obtained as

$$\dot{e} = -ke + \hat{u}_d - u_d = -ke + \mathcal{L}^{-1}\left\{\frac{-\tau s}{\tau s + 1}\right\} * u_d \tag{9}$$

Considering that the reference signal y_m is a step type signal and δ is also a constant, the lumped uncertainty term u_d can be viewed as an unknown step type signal. Consequently, the Laplace transform of u_d can be obtained as (D/s), where D is an unknown constant. Therefore, Eq. (9) can be written as $\dot{e} = -ke - D\exp(-(t/\tau))$. The tracking error is solved via

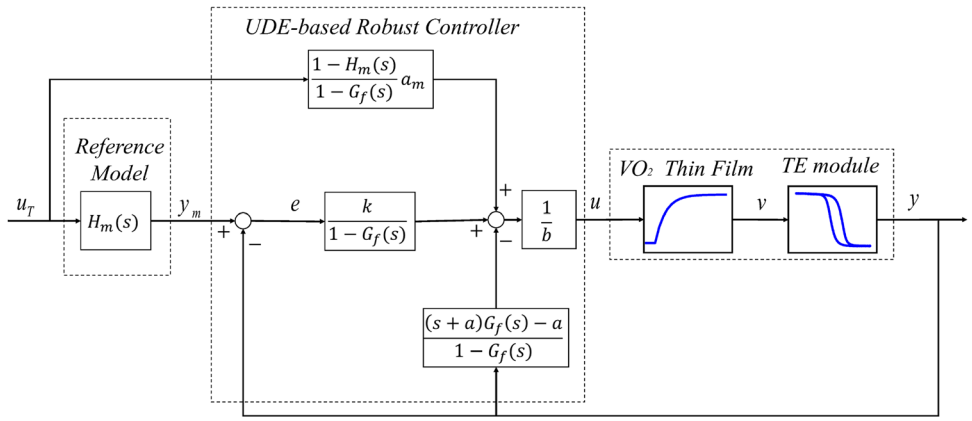

Fig. 5 Block diagram for the closed-loop system

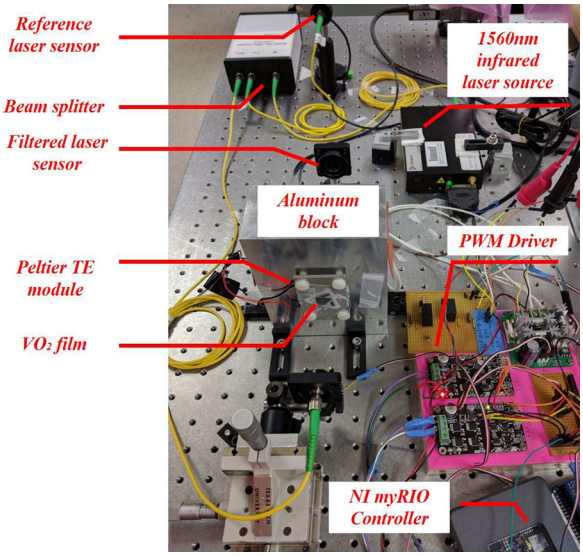

Fig. 6 Experimental platform

$$e = \begin{cases} \left(e(0) + \dfrac{D\tau}{\tau k - 1}\right)\exp(-kt) - \dfrac{D\tau}{\tau k - 1}\exp\left(-\dfrac{t}{\tau}\right), & \tau k \neq 1 \\ (e(0) - Dt)\exp(-kt), & \tau k = 1 \end{cases} \tag{10}$$

In Eq. (10), $e \to 0$ as $t \to \infty$, and the convergence rate of e is determined by k and τ. Larger k and smaller τ can induce the faster convergence. In most cases, where u_d is a constant or varies slowly, the first-order low-pass filter $G_f(s) = (1/(\tau s + 1))$ is good enough to achieve fine control performance. While u_d varies faster or is more complicated, a higher-order filter can be properly designed as reported in Ref. [17].

4 Experimental Validation

4.1 Experimental Setup. Figure 6 shows the experimental setup for the validation, where a thin W-doped VO_2 sample is attached to an aluminum block (used as a heat sink), and a Peltier TE module is used for heating/cooling the VO_2 thin film. In order to minimize possible heating effects, the optical source used in the transmission experiments consisted of a 1560 nm wavelength infrared pulsed laser (pulse width 250 fs, 50 MHz repetition rate, and 18 nm bandwidth). The output of the fiber laser was directed into a beam-splitter and decomposed into 1% and 99% parts. The 1% of output power is used as a reference, and the 99% of output power was coupled into a fiber-optic collimator, which output was used to illuminate the sample at normal incidence. The average power density at the VO_2 sample is determined at $5\,W/cm^2$. This low optical power is not large enough to significantly increase the temperature of the VO_2 film.

In order to verify possible photo-induced heating effects by the laser source, the following experiment was carried out: the VO_2 sample was placed over a heating/cooling stage at different temperatures below the phase transition temperature and the temperature at the sample surface was first measured with a thermal camera with the probe laser off. Then, we repeated the experiment with a $5\,W/cm^2$ power density probe laser illuminating the sample. No noticeable changes in temperature at the VO_2 surface were observed, within the temperature resolution of the thermal camera at $\pm 1\,^{\circ}C$, with either the probe laser on or off.

Thorlabs' PM100 USB optical power sensors are used to detect the reference optical power $P_{ref} = 1\%P_{total}$ and the optical power P_{filter}, which is being filtered by the VO_2 thin film. Then, the optical transmittance is calculated by $y = (P_{filter}/99P_{ref}) \times 100\%$.

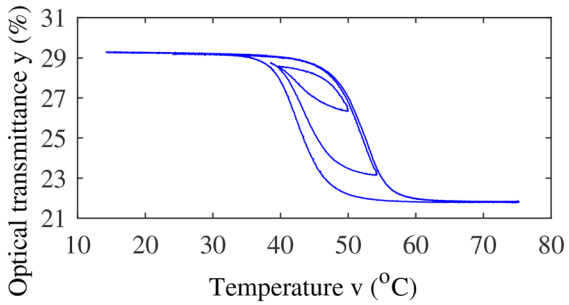

Fig. 7 The measured temperature–transmittance relationship of the VO_2 sample

The Peltier TE module is driven by the pulse width modulation driver, and the control signal is generated by a National Instruments myRIO controller with a sampling time of 1.5 s. Figure 7 shows the hysteresis loops of the measured temperature–transmittance relationship of the VO_2 sample. Following the tuning guideline in Ref. [18], the control parameters in Eq. (8) can be chosen as $a = 0.02$, $b = -5$. The filter $G_f = (1/(\tau s + 1)) = (1/(20s + 1))$, where the time constant $\tau = 20$ is wide enough to make the bandwidth of $G_f(s)$ to cover the spectrum of u_d. The error feedback gain is selected properly large as $k = 1200$.

4.2 Experimental Results

4.2.1 Digital Operation: Acting as a Multiple-State Switch. In this case, the transmittance values of 23%, 25%, and 27% are selected as intermediate operational states, and the reference signal y_m is given as a piecewise continuous function of u_T

$$y_m = \begin{cases} 27\%, & u_T \in [0, 1) \\ 25\%, & u_T \in [1, 2) \\ 23\%, & u_T \in [2, 3] \end{cases} \tag{11}$$

The regulation signal u_T is assumed to vary between 0 and 3 continuously and follows the time profile given as

$$u_T = \begin{cases} \dfrac{3t}{500}, & t \in [0\,s, 500\,s] \\ 3 - \dfrac{3(t - 500)}{500}, & t \in (500\,s, 1000\,s] \end{cases} \tag{12}$$

In this situation, the desired reference signal y_m is settled to 27%, 25%, 23%, 25%, and 27% in sequence and halts at each state for 200 s. Figure 8 shows the phase controlling results. As shown in Fig. 8(*a*), the optical transmittance of VO_2 thin film is successfully regulated to the desired intermediate operational states. The tracking error is plotted in Fig. 8(*b*), where the steady-state error is within 0.1%. The temperature–transmittance (v–y) relationship is depicted in Fig. 8(*c*), and it can be seen that the system output y can be successfully regulated to the desired intermediate operational states, 23%, 25%, and 27%. The $u_T - y$ relationship is then demonstrated in Fig. 8(*d*) as piecewise continuous, instead of hysteretic. The VO_2 device behaves as a multiple-state switch. Figures 8(*e*) and 8(*f*) illustrate the profiles of the sample temperature and the control input voltage, respectively.

4.2.2 Analog Operation: Acting as a Tuning Knob. In this case, the intermediate operational states are selected as a continuous triangular wave between 23% and 27%. Henceforth, the reference signal y_m is a continuous function of u_T

$$y_m = \begin{cases} 27\%, & u_T \in [0, 1) \\ 27\% - \dfrac{4\%}{3}(u_T - 1), & u_T \in [1, 4] \\ 23\%, & u_T \in (4, 5] \end{cases} \tag{13}$$

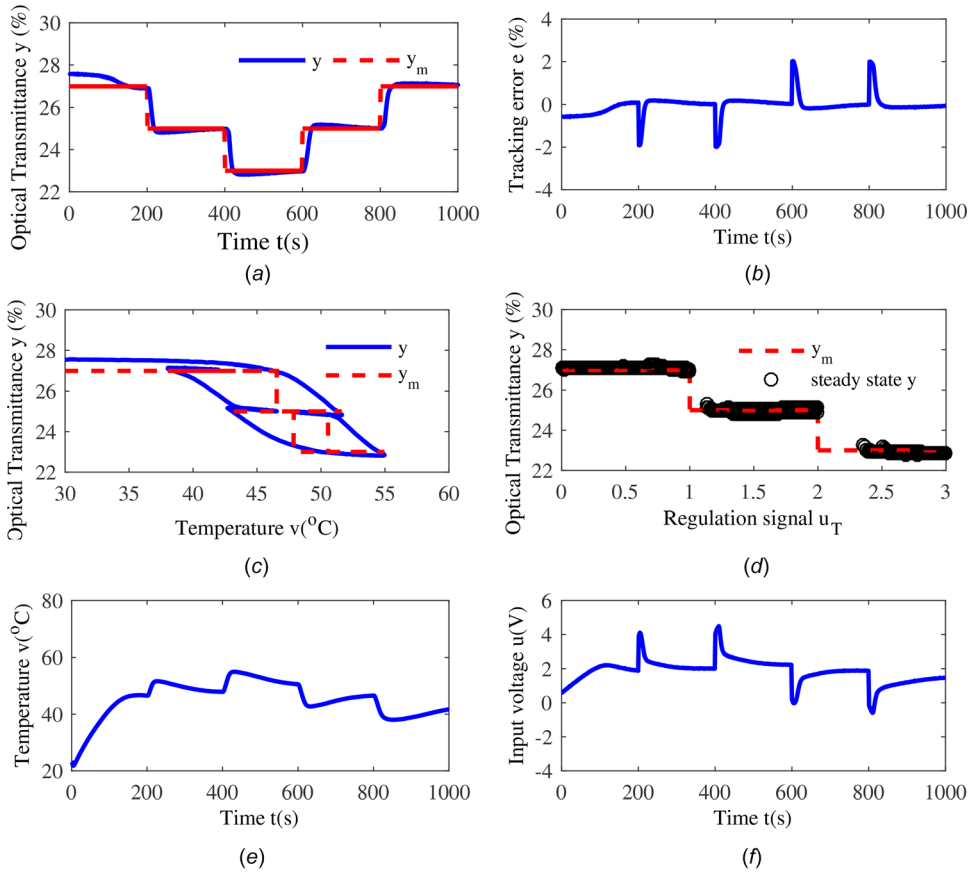

Fig. 8 Digital operation: acting as a multiple-state switch: (*a*) transmittance, (*b*) tracking error, (*c*) *v–y* relationship, (*d*) u_T–*y* relationship, (*e*) temperature, and (*f*) input voltage

The regulation signal u_T varies between 0 and 5 and has the following time profile:

$$u_T = \begin{cases} \dfrac{t}{100}, & t \in [0\,\text{s}, 100\,\text{s}) \\ 1 + \dfrac{3(t-100)}{200}, & t \in [100\,\text{s}, 300\,\text{s}) \\ 4 - \dfrac{3(t-300)}{200}, & t \in [300\,\text{s}, 500\,\text{s}) \\ 1 + \dfrac{3(t-500)}{200}, & t \in [500\,\text{s}, 700\,\text{s}) \\ 4 - \dfrac{3(t-700)}{200}, & t \in [700\,\text{s}, 900\,\text{s}] \\ 1, & t \in (900, 1000] \end{cases} \tag{14}$$

In order to behave like a tuning knob, u_T keeps varying between 1 and 4 with a period of 200 s. The controlling performance is demonstrated in Fig. 9. Figure 9(*a*) demonstrates the phase controlling performance along the triangular wave reference. The steady-state error is also within 0.1%, as shown in Fig. 9(*b*). The temperature–transmittance (*v*–*y*) relationship in Fig. 9(*c*) illustrates the tuned phase trajectory following the reference trajectory properly. Figure 9(*d*) shows the $u_T - y$ relationship as linear. The profiles of the sample temperature and the control input voltage are shown in Figs. 9(*e*) and 9(*f*), respectively.

4.3 Comparison Among Different Controllers. In order to demonstrate the superiority of the proposed control methodology, a comparative study among several approaches is presented. In this case, the reference signal y_m is chosen as a sinusoidal wave with a period of 400 s

$$y_m = \begin{cases} 25, & t \in [0, 100) \\ 25 + 2\sin(0.0157(t-100)), & t \in [100, 900] \\ 25, & t \in (900, 1000] \end{cases} \tag{15}$$

The following approaches are considered:

(1) The proposed UDE-based feedback controller in Sec. 3 (abbreviated in UDE).
(2) The classical PI feedback controller (abbreviated in PI).
(3) The hysteresis inversion-based feedforward controller (abbreviated in FF).
(4) The hysteresis inversion-based feedforward plus the PI feedback controller (abbreviated in FF + PI).

As shown in Fig. 10, the control structure for each approach is presented. It is seen that UDE and PI controllers do not require the hysteresis modeling information, while FF and FF + PI do.

In Figs. 10(*c*) and 10(*d*), both FF and FF + PI use the inverse multiplicative structure to implement the hysteresis compensator [19]. The UDE uses the same control parameters in Sec. 4.1, and the PI controller is chosen as $k_P + (k_I/s)$, $k_P = -400$, $k_I = -100$, where the control gains are tuned manually. The FF + PI inherits the same parameters from PI and FF. The control performance of each approach for tracking a sinusoidal wave (15) is presented in Fig. 11.

As seen in Figs. 11(*a*) and 11(*b*), the qualities of control performance have an order as UDE > FF + PI ≥ PI > FF. Define the relative tracking error as

$$E_r = \frac{\max|y(t_n) - y_m(t_n)|}{\max(y_m) - \min(y_m)} \tag{16}$$

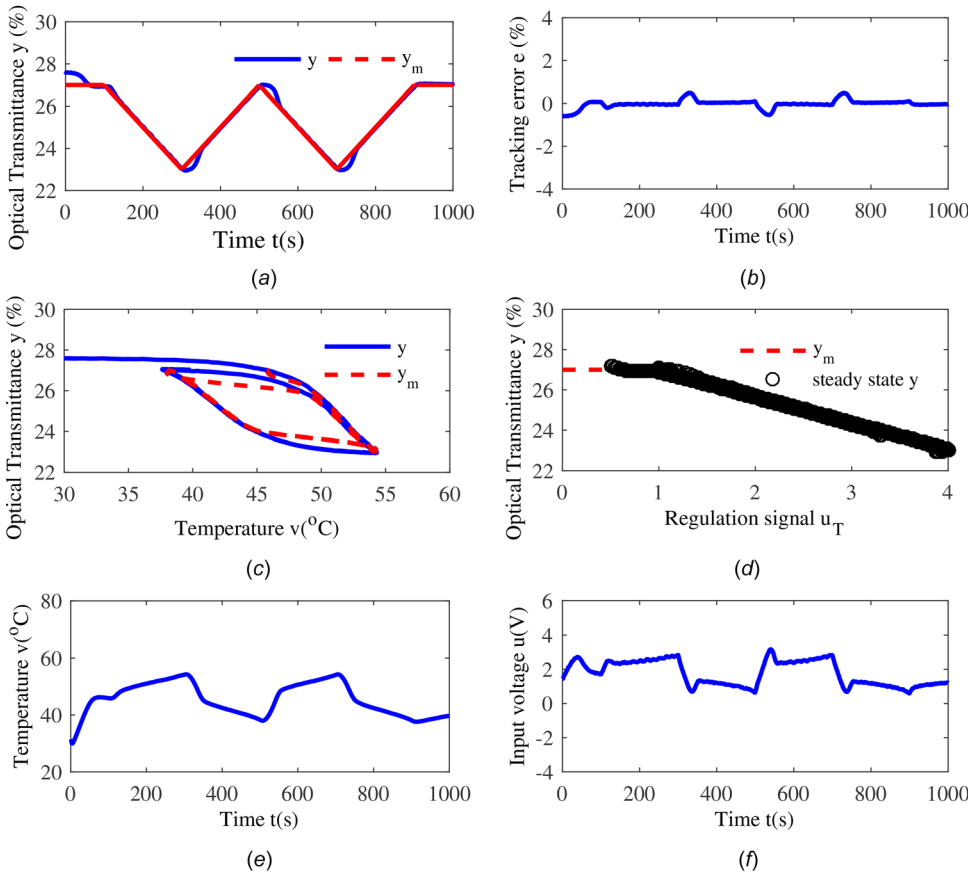

Fig. 9 Analog operation: acting as a tuning knob: (*a*) transmittance, (*b*) tracking error, (*c*) *v–y* relationship, (*d*) u_T–*y* relationship, (*e*) temperature, and (*f*) input voltage

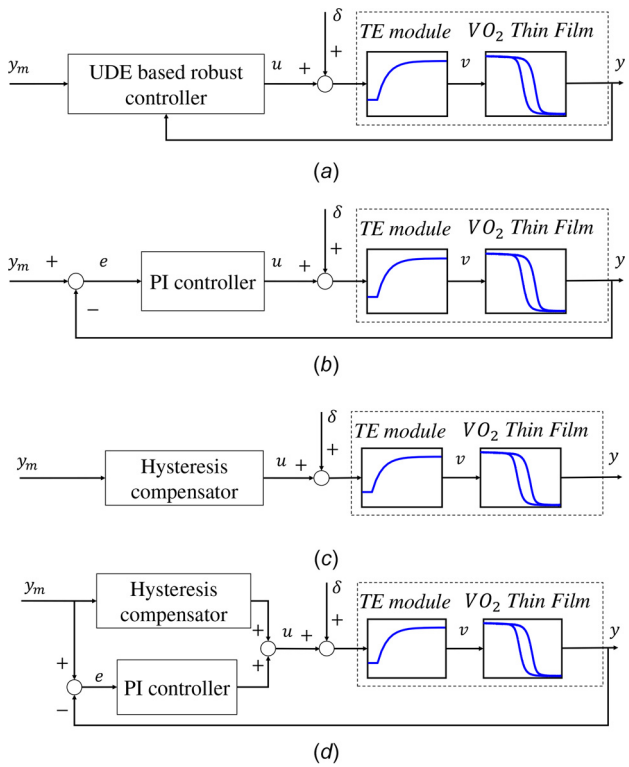

Fig. 10 Different control approaches: (*a*) UDE-based robust feedback controller (UDE), (*b*) PI feedback controller (PI), (*c*) inversion-based FF, and (*d*) inversion-based feedforward plus PI feedback controller (FF + PI)

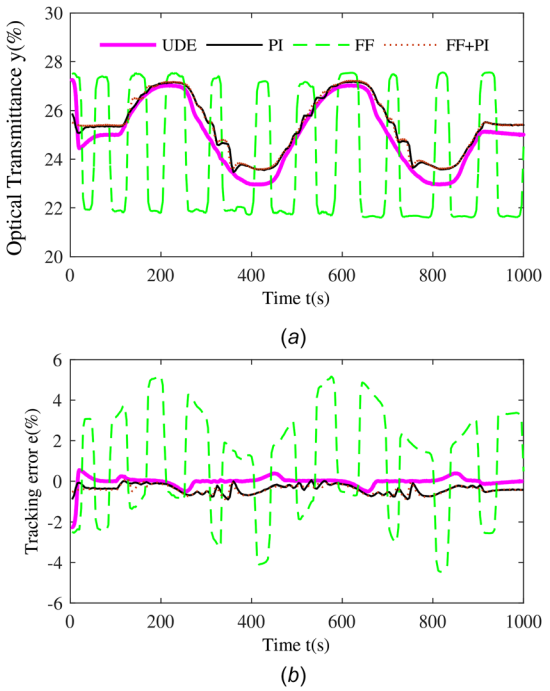

Fig. 11 Comparative results: (*a*) transmittance and (*b*) tracking error

where $y(t_n)$ and $y_m(t_n)$ are the system output and the reference signal at $t = t_n$, respectively. Among all the approaches, UDE has the best control performance, while the relative tracking error is around $0.03\%/4\% = 0.0075$ at the steady-state. The pure feedforward method, FF, completely fails in controlling as it has no tolerance for the modeling mismatches or the external disturbances. The feedback structure is more important in improving the control performance. The PI controller has the simplest structure, but its steady-state error is large, around $0.33\%/4\% = 0.0825$. After adding the inversion-based feedforward term in the control structure, the control performance of PI can be improved to some extent with the relative steady-state error around $0.22\%/4\% = 0.055$. However, the control performance of FF + PI is still worse than UDE.

5 Conclusions

The results in the paper have shown the feasibility of applying the feedback control mechanism to achieve continuous phase controlling of VO_2 films within the full phase transition region. With the excellent performance of the UDE-based robust controller, continuous optical transmittance control for VO_2 films has been achieved. The phase transition of the empowered VO_2 device has been reconfigured by properly selecting a reference model. Thus, such an empowered VO_2 device is of interest in analog applications. Under this control approach, only few system information and the spectrum information of disturbances are needed. The tuning of the control parameters is straightforward, and the implementation of the controller is simpler. The effectiveness of the proposed feedback mechanism has been verified experimentally.

Funding Data

- U.S. National Science Foundation (NSF) (Grant No. CMMI-1728255; Funder ID: 10.13039/100000001).
- U.S. NSF Under an Independent Research and Development Agreement (Funder ID: 10.13039/100000001).

References

[1] Morin, F., 1959, "Oxides Which Show a Metal-to-Insulator Transition at the Neel Temperature," Phys. Rev. Lett., **3**(1), pp. 34–36.

[2] Yang, Z., Ko, C., and Ramanathan, S., 2011, "Oxide Electronics Utilizing Ultrafast Metal-Insulator Transitions," Annu. Rev. Mater. Res., **41**(1), pp. 337–367.

[3] Zhang, J., Merced, E., Sepúlveda, N., and Tan, X., 2014, "Modeling and Inverse Compensation of Nonmonotonic Hysteresis in VO_2-Coated Microactuators," IEEE/ASME Trans. Mechatronics, **19**(2), pp. 579–588.

[4] Bu, Y., Zou, J., Liu, Y., Zhu, Z., Deng, W., Peng, X., and Tang, B., 2017, "Simple and Efficient Synthesis of High-Quality VO_2 Thin Films and Their Application in Vacuum Sensor With Wide Pressure Range," Thin Solid Films, **638**, pp. 420–425.

[5] Gao, Y., Luo, H., Zhang, Z., Kang, L., Chen, Z., Du, J., Kanehira, M., and Cao, C., 2012, "Nanoceramic VO_2 Thermochromic Smart Glass: A Review on Progress in Solution Processing," Nano Energy, **1**(2), pp. 221–246.

[6] Malarde, D., Powell, M. J., Quesada-Cabrera, R., Wilson, R. L., Carmalt, C. J., Sankar, G., Parkin, I. P., and Palgrave, R. G., 2017, "Optimized Atmospheric-Pressure Chemical Vapor Deposition Thermochromic VO_2 Thin Films for Intelligent Window Applications," ACS Omega, **2**(3), pp. 1040–1046.

[7] Stefanovich, G., Pergament, A., and Stefanovich, D., 2000, "Electrical Switching and Mott Transition in VO_2," J. Phys. Condens. Matter, **12**(41), pp. 8837–8845.

[8] Bonora, S., Bortolozzo, U., Residori, S., Balu, R., and Ashrit, P., 2010, "Mid-IR to Near-IR Image Conversion by Thermally Induced Optical Switching in Vanadium Dioxide," Opt. Lett., **35**(2), pp. 103–105.

[9] Hoque, M. N. F., Karaoglan-Bebek, G., Holtz, M., Bernussi, A. A., and Fan, Z., 2015, "High Performance Spatial Light Modulators for Terahertz Applications," Opt. Commun., **350**, pp. 309–314.

[10] Jian, J., Wang, X., Li, L., Fan, M., Zhang, W., Huang, J., Qi, Z., and Wang, H., 2017, "Continuous Tuning of Phase Transition Temperature in VO_2 Thin Films on c-Cut Sapphire Substrates Via Strain Variation," ACS Appl. Mater. Interfaces, **9**(6), pp. 5319–5327.

[11] Karaoglan-Bebek, G., Hoque, M. N. F., Holtz, M., Fan, Z., and Bernussi, A. A., 2014, "Continuous Tuning of W-Doped VO_2 Optical Properties for Terahertz Analog Applications," Appl. Phys. Lett., **105**(20), p. 201902.

[12] Annasiwatta, A. W. C. D., Chen, J., Berg, J. M., Bernussi, A., Fan, Z., and Ren, B., 2016, "Modeling Hysteresis in Vanadium Dioxide Thin Films," Proceedings of American Control Conference, Boston, MA, pp. 6905–6910.

[13] Janaideh, M. A., Rakheja, S., and Su, C.-Y., 2011, "An Analytical Generalized Prandtl-Ishlinskii Model Inversion for Hysteresis Compensation in Micropositioning Control," IEEE/ASME Trans. Mechatronics, **16**(4), pp. 734–744.

[14] Zhang, J., Torres, D., Ebel, J. L., Sepúlveda, N., and Tan, X., 2016, "A Composite Hysteresis Model in Self-Sensing Feedback Control of Fully Integrated VO_2 Microactuators," IEEE/ASME Trans. Mechatronics, **21**(5), pp. 2405–2417.

[15] Zhong, Q.-C., and Rees, D., 2004, "Control of Uncertain LTI Systems Based on an Uncertainty and Disturbance Estimator," ASME J. Dyn. Syst. Meas. Control, **126**(4), pp. 905–910.

[16] Dai, J., Ren, B., and Zhong, Q.-C., 2018, "Uncertainty and Disturbance Estimator-Based Backstepping Control for Nonlinear Systems With Mismatched Uncertainties and Disturbances," ASME J. Dyn. Syst. Meas. Control, **140**(12), p. 121005.

[17] Ren, B., Zhong, Q.-C., and Dai, J., 2017, "Asymptotic Reference Tracking and Disturbance Rejection of UDE-Based Robust Control," IEEE Trans. Ind. Electron., **64**(4), pp. 3166–3176.

[18] Ren, B., Dai, J., and Zhong, Q.-C., 2019, "UDE-Based Robust Output Feedback Control With Applications to a Piezoelectric Stage," IEEE Trans. Ind. Electron. epub.

[19] Li, Z., Su, C.-Y., and Chai, T., 2014, "Compensation of Hysteresis Nonlinearity in Magnetostrictive Actuators With Inverse Multiplicative Structure for Preisach Model," IEEE Trans. Autom. Sci. Eng., **11**(2), pp. 613–619.